

Growth rate of crystalline ice and the diffusivity of supercooled water from 126 to 262 K

Yuntao Xu^a, Nikolay G. Petrik^a, R. Scott Smith^a, Bruce D. Kay^{a,1}, and Greg A. Kimmel^{a,1}

^aChemical Physics & Analysis, Physical Sciences Division, Physical & Computational Sciences Directorate, Pacific Northwest National Laboratory, Richland, WA 99352

Edited by Pablo G. Debenedetti, Princeton University, Princeton, NJ, and approved November 20, 2016 (received for review July 12, 2016)

Understanding deeply supercooled water is key to unraveling many of water's anomalous properties. However, developing this understanding has proven difficult due to rapid and uncontrolled crystallization. Using a pulsed-laser-heating technique, we measure the growth rate of crystalline ice, $G(T)$, for $180\text{ K} < T < 262\text{ K}$, that is, deep within water's "no man's land" in ultrahigh-vacuum conditions. Isothermal measurements of $G(T)$ are also made for $126\text{ K} \leq T \leq 151\text{ K}$. The self-diffusion of supercooled liquid water, $D(T)$, is obtained from $G(T)$ using the Wilson-Frenkel model of crystal growth. For $T > 237\text{ K}$ and $P \sim 10^{-8}\text{ Pa}$, $G(T)$ and $D(T)$ have super-Arrhenius ("fragile") temperature dependences, but both cross over to Arrhenius ("strong") behavior with a large activation energy in no man's land. The fact that $G(T)$ and $D(T)$ are smoothly varying rules out the hypothesis that liquid water's properties have a singularity at or near 228 K at ambient pressures. However, the results are consistent with a previous prediction for $D(T)$ that assumed no thermodynamic transitions occur in no man's land.

supercooled water | self-diffusion | crystallization kinetics | dynamic crossover

Water is not a typical liquid, and its unusual properties have been discussed by many authors (1–13). Anomalies are observed in thermodynamic response functions (such as the isobaric heat capacity and the isothermal compressibility) and dynamic properties (such as diffusion, viscosity, and dielectric relaxation) over a wide range of pressures, P , and temperatures, T . These anomalies become more pronounced for supercooled water, and it is generally believed that the unusual properties arise as water adopts a more ice-like structure as the temperature decreases. However, the underlying reasons are fiercely debated (5, 11, 14–17). At ambient pressures, many of the anomalous properties appear to diverge at a temperature, T_s , around 228 K leading to the "stability-limit conjecture" in which the liquid becomes unstable below T_s (2). Several other models have been proposed to explain the thermodynamic anomalies including the liquid-liquid critical point model (3), the critical-point free scenario (18), and the singularity-free hypothesis (19). However, it is noteworthy that both thermodynamic and dynamic properties apparently diverge at $\sim T_s$ (1, 2). To explain the similarities in the thermodynamics and dynamics, Adam-Gibbs theory is attractive because it connects changes in the entropy of a liquid to its dynamics (20). Using this theory, Starr et al. (6) predicted that the self-diffusion of water, $D(T)$, undergoes a dynamic crossover from super-Arrhenius to Arrhenius behavior (often called a "fragile-to-strong" transition) at temperatures just below the homogeneous nucleation temperature, T_H , at $\sim 235\text{ K}$. However, purely dynamical explanations have also been proposed (5, 21).

Differentiating between various theories has proven difficult because the onset of rapid crystallization at T_H has prevented experiments below this point (5, 22). Another approach involves heating low-density amorphous (LDA) ice above its glass transition temperature ($\sim 136\text{ K}$) before crystallization at $\sim 150\text{ K}$ (5, 10). The heretofore-inaccessible temperature range between ~ 150 and 235 K at ambient pressures is known as "no man's land" (5, 23). Experiments on water confined to nanoscale drops provide entry

into no man's land (24, 25) but are complicated by interfacial effects (10). Considerable insight has also been gained by exploring water's unusual properties over a wide range of pressures (3, 5, 7, 23).

Here, we report the growth rate of crystalline ice, $G(T)$, using a pulsed-heating technique (26) for $181\text{ K} \leq T < 262\text{ K}$ and measured isothermally for $126\text{ K} \leq T \leq 151\text{ K}$. Because $G(T)$ is proportional to $D(T)$ (27–29), we also determine $D(T)$. For $T > 235\text{ K}$, we reproduce the previously measured super-Arrhenius behavior (30). For $180\text{ K} < T < 235\text{ K}$, $G(T)$ and $D(T)$ cross over to Arrhenius dependences with large activation energies and pre-factors. For $126\text{ K} \leq T < 180\text{ K}$, $G(T)$ and $D(T)$ are also Arrhenius-like but with lower activation energies. These results for $D(T)$, which are inconsistent with a singularity at or near T_s , agree with the prediction of a fragile-to-strong crossover using the thermodynamic properties of water and the Adam-Gibbs theory (6, 20).

Results

Fig. 1A shows a schematic of the pulsed-heating experiments (26). The crystalline ice growth rates were measured for layered ice/water samples (*Sample Preparation* and Figs. S1 and S2). First, 75-monolayer (ML) films of polycrystalline ice (CI) were prepared on Pt(111) in ultrahigh vacuum. Next, 25-ML films of amorphous solid water (ASW) were deposited to create metastable, layered CI-ASW films. To enhance the sensitivity of the measurements, the CI films were composed of pure H_2O , whereas the ASW layers had $\sim 9.5\%$ HDO in H_2O . With the steady-state temperature set at 90 K , the platinum substrate was heated with IR pulses from a Nd:YAG laser ($\lambda = 1,064\text{ nm}$, $\sim 10\text{ ns}$, $1\text{--}10\text{ Hz}$). Facile heat transfer from the substrate raised the temperature of the adsorbed water

Significance

Water is ubiquitous, but its physical properties are anomalous compared with most liquids. Because the anomalies become enhanced upon cooling, understanding the behavior of deeply supercooled water is critical. Unfortunately, experiments below $\sim 236\text{ K}$ at ambient pressure are difficult due to uncontrolled crystallization. Using a pulsed-laser-heating technique, we have determined the crystalline-ice growth rate and liquid-water diffusivity for temperatures between 180 and 262 K in ultrahigh-vacuum conditions. The fact that both of these quantities are smoothly varying rules out the hypothesis that water's properties have a singularity at or near 228 K . However, the results are consistent with a previous prediction for the diffusivity that assumed no thermodynamic transitions occur in the supercooled region.

Author contributions: N.G.P., R.S.S., B.D.K., and G.A.K. designed research; Y.X. performed research; Y.X., B.D.K., and G.A.K. analyzed data; and Y.X., N.G.P., R.S.S., B.D.K., and G.A.K. wrote the paper.

The authors declare no conflict of interest.

This article is a PNAS Direct Submission.

¹To whom correspondence may be addressed. Email: gregory.kimmel@pnl.gov or bruce.kay@pnl.gov.

This article contains supporting information online at www.pnas.org/lookup/suppl/doi:10.1073/pnas.1611395114/-DCSupplemental.

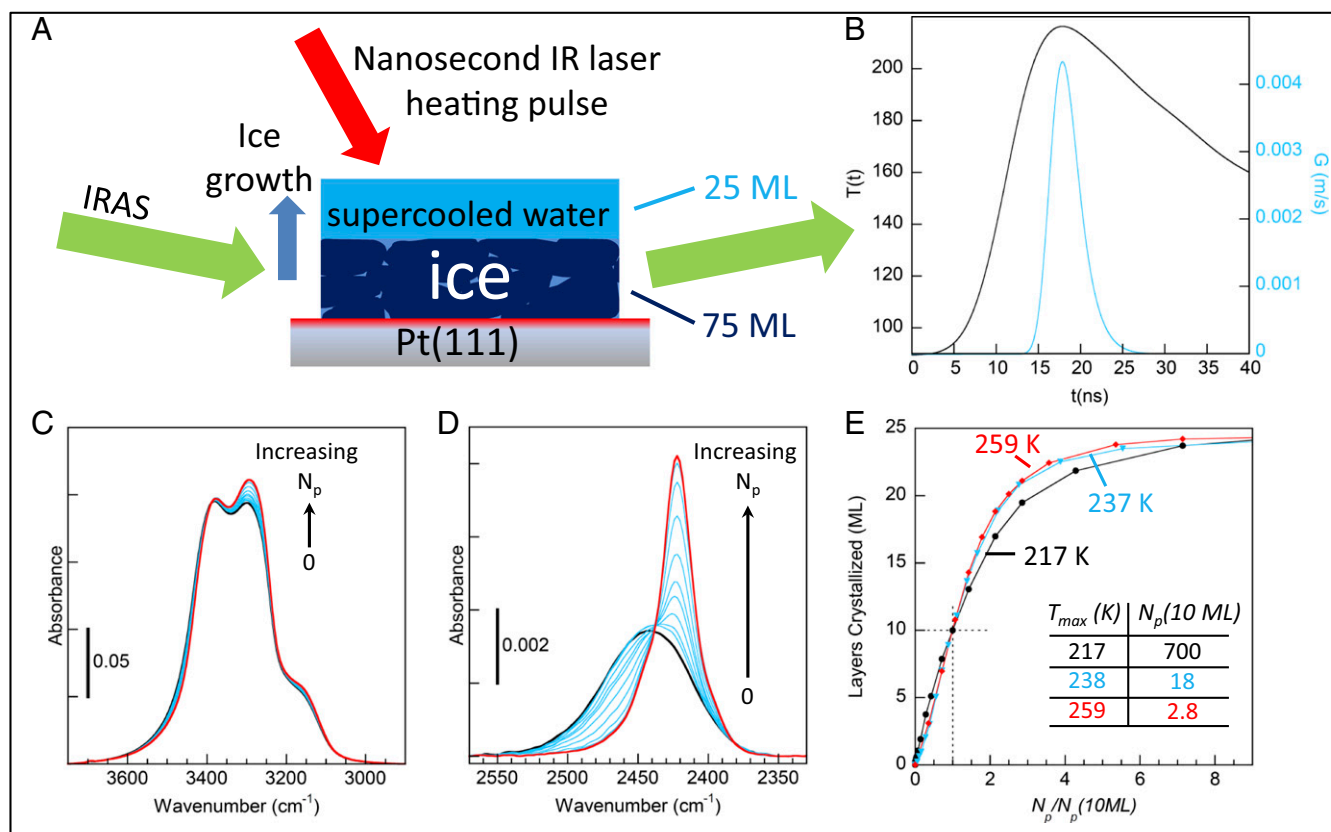


Fig. 1. (A) Schematic of the experiments. Nanoscale films were heated with a laser pulse that raised the temperature for ~ 20 ns, creating a film of supercooled water on top of ice. Ice growth that occurred due to the pulsed heating was measured with IRAS. (B) $T(t)$ calculated for $T_{\max} = 217$ K (black) and the corresponding $G(T)$ that matches the observations (blue). (C and D) IRAS spectra for an as-grown film (black), at intermediate stages of ice growth (blue), and after crystallization is complete (red). Both the OH-stretch (C) and the isolated HDO-stretch (D) regions show the crystallization. (E) The number of MLs of the initially amorphous layers crystallized vs. the number of heat pulses, N_p , for $T_{\max} = 217$, 237, and 259 K. To facilitate comparison, N_p has been normalized by the number of pulses required to crystallize 10 ML at each temperature.

films to their maximum value, T_{\max} , in ~ 20 ns, and subsequent diffusion of heat into the platinum rapidly cooled the samples back to cryogenic temperatures in between pulses. The black line in Fig. 1B shows the calculated temperature, $T(t)$, for a typical heat pulse. $T(t)$ was calibrated by measuring the water desorption per pulse from the films after they had crystallized (*Temperature Calibration*) (26).

The rapid heating transforms the ASW layer into supercooled liquid water with a concomitant increase in the diffusion leading to CI growth at the ice–water interface at the rate, $G(T)$ (e.g., Fig. 1B, blue line). Infrared reflection absorption spectroscopy (IRAS) was used to monitor the ice growth. Note that the IRAS spectra were acquired at 90 K after a specified number of heat pulses, N_p , had been applied to the sample. Fig. 1C shows how the OH-stretch region of the IRAS spectra evolves as the film crystallizes. By construction, HDO molecules are found only in the (initially) liquid layer, and, as a result, the crystallization of this layer is more readily apparent in the OD-stretch region (Fig. 1D). The amount of ice in the films can be determined by fitting the IRAS spectra to a linear combination of the initial and final spectra (Fig. S3). Fig. 1E shows the ice growth vs. the (normalized) number of laser pulses for $T_{\max} = 217$, 237, and 259 K. For all three temperatures, the crystallization increases approximately linearly vs. N_p . (The experimental factors contributing to the deviations from linearity are discussed in *Determination of Growth Rates from IRAS Spectra*.) Note that there is no qualitative change in the results even at 217 K, which is ~ 18 K below T_H . Several control experiments show that ice nucleation within the liquid layer or at the liquid–vacuum interface is not significant for these experiments (*Ice Nucleation*,

and Figs. S4 and S5). We have also measured $G(T)$ for films with different thicknesses of both the CI layer (50–150 ML) and the liquid-water layer (15–75 ML) and found that $G(T)$ is unchanged. At temperatures near the melting point, a quasiliquid layer forms on the surface of CI (31). However, the fact that the measured growth rates do not depend on the initial thickness of the liquid-water layer suggests that a quasiliquid layer does not influence the results presented here. This conclusion also agrees with previous results that indicate that the quasiliquid layer should be less than 1 nm thick for $T < 263$ K (31). Because our experiments produce macroscopically flat films, curvature effects can also be ignored. Collectively, these points indicate that our measurements are germane to bulk supercooled water.

From experiments like those shown in Fig. 1E, the amount of ice growth per heat pulse, $\tilde{G}(T_{\max})$, can be determined (Fig. 2, black circles). At the highest temperatures, $\tilde{G}(T_{\max})$ changes relatively slowly with temperature, whereas for $T < 235$ K, $\tilde{G}(T_{\max})$ decreases very quickly. An Arrhenius fit to the data yields an activation energy of ~ 76 kJ/mol (Fig. 2, dashed blue line). $\tilde{G}(T_{\max})$ is related to $G(T)$ by an integral equation that explicitly treats the temperature as function of time, $T(t)$, at the ice/liquid interface during each heat pulse:

$$\tilde{G}(T_{\max}) \equiv \int_{\text{pulse}} G(T(t)) dt. \quad [1]$$

Because $T(t)$ is known (*Temperature Calibration*) (26), $\tilde{G}(T_{\max})$ can be calculated using trial functions for $G(T)$ in Eq. 1 and then

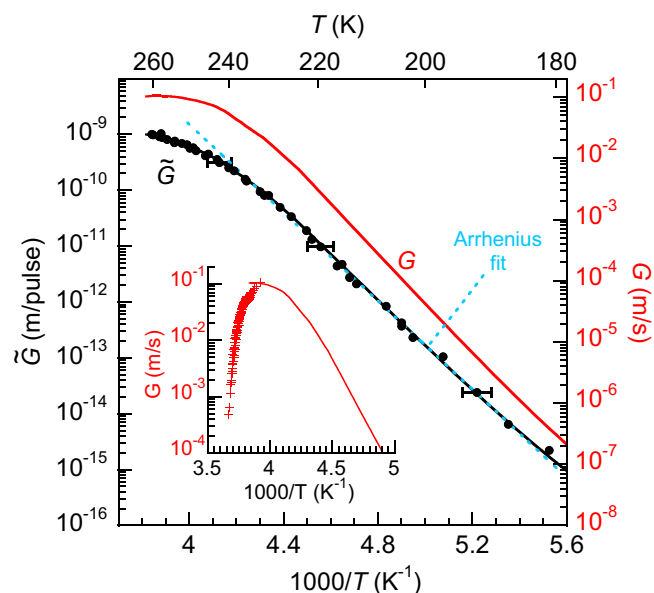


Fig. 2. $\bar{G}(T_{\max})$ and $G(T)$ vs. inverse temperature. The black circles show the measured values for $\bar{G}(T_{\max})$. $\bar{G}(T_{\max})$ exhibits Arrhenius behavior (~ 76 kJ/mol) for $T_{\max} < 235$ K (blue dashed line). The measured growth rates are the integrals of $G(T)$ over a heat pulse, $T(t)$, with a maximum temperature, T_{\max} (Eq. 1). The red line shows a form of $G(T)$ that reproduces the results of the pulsed-heating experiment (black line). The *Inset* compares previous measurements of $G(T)$ for macroscopic samples (32) (crosses) to the current experiments on nanoscale water films (red line). For $\bar{G}(T_{\max})$, the vertical size of the symbols is representative of the uncertainty in the measurements ($\pm 20\%$). Horizontal error bars, which show the lateral distribution of temperatures on the sample during the heat pulses, are shown for a few points.

compared with the experimentally measured values. Fig. 2 shows a form of $G(T)$ that reproduces the observed $\bar{G}(T_{\max})$ (Fig. 2, red and black lines, respectively).

Previous measurements of $G(T)$ have been made on macroscopic samples over a relatively small temperature range near the melting point (32–34), or on nanoscale films at cryogenic temperatures (35). At the melting point, $G(T) = 0$ and at temperatures just below this, $G(T)$ rapidly increases with decreasing temperature as the thermodynamic driving force for crystallization increases (27–29). As discussed below, $G(T)$ is expected to go through a maximum and then decrease at even lower temperatures due to a decrease in $D(T)$. It is important to note that, for macroscopic samples, the heat of fusion that is released upon crystallization and subsequent heat transfer from the ice/water interface limits the minimum temperature that is achieved at the interface (36). The local heating at the ice/water interface has precluded observation of the expected decrease in $G(T)$ with decreasing temperature in macroscopic samples. These effects are less important in the nanoscale films used here (*Latent Heat of Fusion* and Fig. S6), and the decrease in $G(T)$ expected at lower temperatures is clearly observed (Fig. 2). Nonetheless, the magnitude of $G(T)$ determined for macroscopic samples agrees reasonably well with the current results at comparable temperatures (Fig. 2, *Inset*).

Molecular dynamics simulations have been used to investigate the growth of CI in contact with the supercooled liquid with a variety of water models (37–43). An advantage of the simulations is that they can be done using various techniques to remove the latent heat generated by the crystallization (39, 40). As a result, $G(T)$ can be investigated as a function of the (known) interface temperature. In this sense, the calculations can be more directly related to our measurements of $G(T)$ than to earlier measurements of $G(T)$ on macroscopic samples, and several simulations have observed a maximum in $G(T)$ (38, 39, 42, 44). For example, simulations with

TIP4P/ice, which has a melting point of 270 K, observed a maximum at 260 K and found that $G(T)$ decreased by $\sim 50\%$ by 245 K (39). Both of these results are in qualitative agreement with our measurements.

For T less than ~ 180 K, $G(T)$ is small enough to preclude measuring it via pulsed heating. However, $G(T)$ can be measured directly in isothermal experiments at even lower temperatures (*Isothermal Measurements*) (35). Fig. 3 shows $G(T)$ measured isothermally for 126 K $\leq T \leq 151$ K (red diamonds). The figure also displays the pulsed-heating data (red circles), which has been scaled for comparison (*Isothermal Measurements*). Collectively, these data span 11 orders of magnitude in $G(T)$. It can be divided into three regions: (i) for $T > 235$ K, $G(T)$ varies slowly with temperature but is clearly non-Arrhenius; (ii) for ~ 180 K $< T < 235$ K, $G(T)$ exhibits Arrhenius behavior with an activation energy of ~ 76 kJ/mol; (iii) for $T \leq 151$ K, $G(T)$ is also Arrhenius but with a lower activation energy of ~ 47 kJ/mol. In Fig. 3, for $T < 225$ K, the red line (solid and dashed), which is the sum of two Arrhenius functions with activation energies appropriate for the intermediate- and low-temperature regions, fits the data over that entire temperature range and suggests that the low-temperature data matches smoothly with $G(T)$ determined from the pulsed-heating measurements.

Although $G(T)$ displayed in Figs. 2 and 3 is interesting in its own right, crystal growth is also intimately related to dynamics occurring in the supercooled liquid. In particular, crystal growth at a liquid/solid interface can be decomposed into a thermodynamic and a kinetic component (27, 28, 45). The thermodynamic component reflects the (net) probability that molecules from the liquid attach to the crystal. The kinetic component is related to the mobility of molecules at the liquid/solid interface, and it is often found that the growth rate is proportional to the diffusivity in the liquid (46, 47).

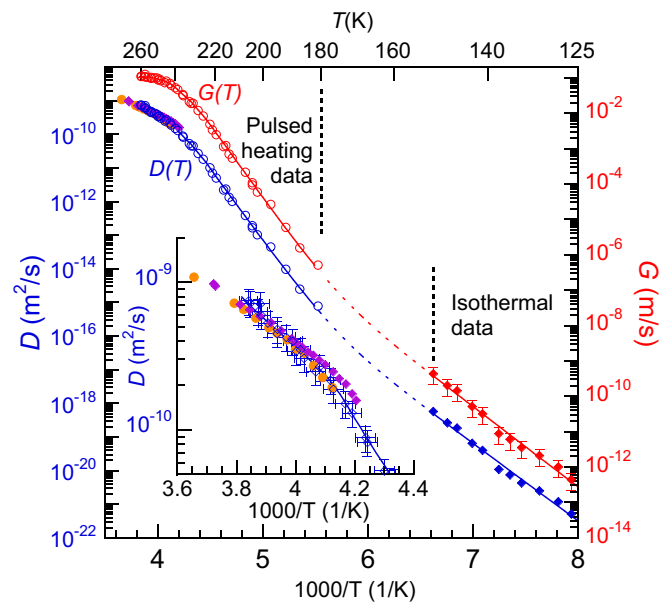


Fig. 3. $D(T)$ and $G(T)$ vs. inverse temperature. For $T \leq 151$ K, $G(T)$ was measured isothermally (red diamonds). The red circles show $\bar{G}(T_{\max})$ scaled to facilitate comparison with the isothermal data. For the region where no data are available, the red dashed line shows a possible form of $G(T)$ as the sum of two Arrhenius functions fit to the data on either side of that region. $D(T)$ (blue line) was determined from $G(T)$ (red line) using the Wilson–Frenkel model. The blue circles and diamonds show the corresponding experimental values for $D(T)$ converted from $G(T)$ via the Wilson–Frenkel model. The orange circles and purple diamonds show previous measurements of $D(T)$ (30, 57). (*Inset*) Expanded view of $D(T)$ near the melting point. The values of $D(T)$ extracted from the pulsed-heating experiments agree with the previously measured values within the uncertainties.

Therefore, our measurements of $G(T)$ can provide valuable insight into the dynamics of supercooled liquid water over a wide temperature range. When the temperature is well below the melting point and the thermodynamic driving force for crystallization is large, the growth rate can be described by the Wilson–Frenkel model:

$$G(T) = (D(T)/\alpha)[1 - \exp(-\Delta G_h(T)/k_b T)], \quad [2]$$

where $\Delta G_h(T)$ is the difference in free energy between the liquid and crystalline phases and α is a constant (27–29). More information on the Wilson–Frenkel model is given in *Wilson–Frenkel Growth Model*. Because $D(T)$ and $\Delta G_h(T)$ are known for $T > 238$ K, we can use our measured $G(T)$ to determine α via Eq. 2 (Fig. S7). At lower temperatures where other techniques for measuring $D(T)$ fail, it can be calculated using Eq. 2 and the measured $G(T)$ (46). The blue line in Fig. 3 shows $D(T)$ calculated with this procedure. Above 238 K, it agrees with known values of $D(T)$ (Fig. 3, *Inset*), whereas at lower temperatures, $\Delta G_h(T)$ is weakly temperature-dependent and thus $D(T)$ closely tracks $G(T)$. There are several noteworthy aspects to these results. First, a power-law fit with a singularity at or near 228 K will not fit either $G(T)$ or $D(T)$ (Fig. S8). Thus, the stability-limit conjecture is incompatible with the current results. Second, the current results for $D(T)$ are incompatible with Vogel–Fulcher–Tammann (VFT) fits such as those used by Price et al. (30) and Smith and Kay (48) (Fig. S8). Instead, $D(T)$ exhibits a similar three-region temperature dependence as discussed above for $G(T)$. Based on the activation energy in the low-temperature region, the fragility index at the glass transition temperature ($T_g \sim 136$ K) is ~ 18 , which is consistent with previous measurements and corresponds to an extremely strong liquid (49).

Discussion

Although using growth rates of the crystalline phase to extract the diffusivity in the liquid phase often works well (46, 47), it also fails in several cases, particularly near the glass transition temperature (50, 51). For example, the growth rate for tris-naphthylbenzene (TNB) tracks the self-diffusion at high temperatures but leads to an overestimate of it by approximately an order of magnitude near T_g (50). A similar level of uncertainty might apply for $D(T)$ shown in Fig. 3, particularly for the isothermal measurements at $T \leq 151$ K. Another potential issue with the Wilson–Frenkel model is related to the type of diffusion, namely, translational or rotational, that is involved in the ice growth. Although it is likely that both are involved, the relative importance of these, particularly near T_g , is currently debated (52, 53). On the other hand, the qualitative features displayed for $D(T)$ —no singularity in the temperature dependence and a fragile-to-strong crossover at ~ 235 K—are unlikely to be changed by any specific shortcomings of the Wilson–Frenkel model.

The complicated form of $D(T)$ shown in Fig. 3 is qualitatively similar to a prediction by Starr et al. (6). Assuming a thermodynamically reversible connection between supercooled water and LDA, they used the entropy, specific heat, and enthalpy of water at 150 and 236 K to estimate the excess entropy, $S_{ex}(T)$, and the configurational entropy, $S_{conf}(T)$, at intermediate temperatures, and then used Adam–Gibbs theory to calculate $D(T)$. With this

approach, they predicted a fragile-to-strong transition (or dynamic crossover) just below 236 K and a second crossover at ~ 187 K to a lower activation energy, both of which agree with the current results. Fragile-to-strong crossovers have also been observed in molecular dynamics simulations at or near the corresponding maxima in C_p as expected from Adam–Gibbs theory (6, 7). The second crossover at ~ 180 K, which is seen in both $G(T)$ and $D(T)$, might be associated with changes in the hydrogen-bonding network of the liquid water. For example, molecular dynamics simulations suggest that the average number of bonds, which is less than four at higher temperatures, approaches four at lower temperatures (54). Thus, one possibility is that the larger apparent activation energy for $T > 180$ K is associated with the mobility in the “defective” liquid and the decreasing number of bonds with increasing temperature. The smaller activation energy found for $T < 180$ K would then be associated with diffusion of molecules in a “fully” hydrogen-bonded liquid (i.e., with a fixed number of bonds).

The success of the Adam–Gibbs prediction for $D(T)$ supports the hypothesis that the unusual thermodynamics of liquid water are also responsible for its dynamic anomalies. Our results appear to be consistent with either the critical-point-free scenario or a liquid–liquid critical point at positive pressures, as both are consistent with a continuous change in entropy across no man’s land. However, because the current experiments are continuous in $G(T)$ and $D(T)$, they provide no evidence for a liquid–liquid transition line extending to negative pressures (55). At low temperatures, our $D(T)$ is considerably larger than the predictions of Starr et al. (6) However, as they noted, this is likely due to the breakdown of the Stokes–Einstein relationship, which is frequently observed for deeply supercooled liquids (56).

Conclusions

In summary, using a recently developed laser-heating technique, we have measured the growth rate of CI, $G(T)$, across a large temperature range of no man’s land at low pressure. When these data are analyzed using the venerable Wilson–Frenkel theory of crystal growth, we are able to extract the self-diffusion coefficient, $D(T)$, for supercooled water over the temperature range from 126 to 262 K. Over this range, $G(T)$ and $D(T)$ smoothly vary by ~ 11 orders of magnitude with no evidence of a singularity. Instead, they exhibit three characteristic temperature dependencies clearly indicating a fragile-to-strong crossover at ~ 233 K and a “strong-to-stronger” crossover at ~ 180 K, which are qualitatively similar to an earlier prediction based on Adam–Gibbs theory (6). This approach affords the opportunity to explore deeply supercooled liquids in regions of the phase diagram that were previously inaccessible due to rapid crystallization.

ACKNOWLEDGMENTS. This work was supported by the US Department of Energy, Office of Science, Office of Basic Energy Sciences, Division of Chemical Sciences, Geosciences, and Biosciences. Pacific Northwest National Laboratory (PNNL) is a multiprogram national laboratory operated for Department of Energy by Battelle. The research was performed using Environmental Molecular Sciences Laboratory, a national scientific user facility sponsored by the Department of Energy’s Office of Biological and Environmental Research and located at PNNL.

- Speedy RJ, Angell CA (1976) Isothermal compressibility of supercooled water and evidence for a thermodynamic singularity at -45 C. *J Chem Phys* 65:851–858.
- Speedy RJ (1982) Stability-limit conjecture. An interpretation of the properties of water. *J Chem Phys* 86:982–991.
- Poole PH, Sciortino F, Essmann U, Stanley HE (1992) Phase behavior of metastable water. *Nature* 360(6402):324–328.
- Scala A, Starr FW, La Nave E, Sciortino F, Stanley HE (2000) Configurational entropy and diffusivity of supercooled water. *Nature* 406(6792):166–169.
- Debenedetti PG (2003) Supercooled and glassy water. *J Phys Condens Matter* 15(45):R1669–R1726.
- Starr FW, Angell CA, Stanley HE (2003) Prediction of entropy and dynamic properties of water below the homogeneous nucleation temperature. *Physica A* 323: 51–66.
- Xu L, et al. (2005) Relation between the Widom line and the dynamic crossover in systems with a liquid–liquid phase transition. *Proc Natl Acad Sci USA* 102(46): 16558–16562.
- Kumar P, et al. (2007) Relation between the Widom line and the breakdown of the Stokes–Einstein relation in supercooled water. *Proc Natl Acad Sci USA* 104(23): 9575–9579.
- Mallamace F, et al. (2008) NMR evidence of a sharp change in a measure of local order in deeply supercooled confined water. *Proc Natl Acad Sci USA* 105(35): 12725–12729.
- Angell CA (2008) Insights into phases of liquid water from study of its unusual glass-forming properties. *Science* 319(5863):582–587.
- Limmer DT, Chandler D (2011) The putative liquid–liquid transition is a liquid–solid transition in atomistic models of water. *J Chem Phys* 135(13):134503.

12. Palmer JC, et al. (2014) Metastable liquid-liquid transition in a molecular model of water. *Nature* 510(7505):385–388.
13. Nilsson A, Pettersson LGM (2015) The structural origin of anomalous properties of liquid water. *Nat Commun* 6:8998.
14. Chandler D (2016) Metastability and no criticality. *Nature* 531(7593):E1–E2.
15. Johari GP, Teixeira J (2015) Thermodynamic analysis of the two-liquid model for anomalies of water, HDL-LDL fluctuations, and liquid-liquid transition. *J Phys Chem B* 119(44):14210–14220.
16. Palmer JC, et al. (2016) Palmer et al. reply. *Nature* 531(7593):E2–E3.
17. Smallemburg F, Sciortino F (2015) Tuning the liquid-liquid transition by modulating the hydrogen-bond angular flexibility in a model for water. *Phys Rev Lett* 115(1):015701.
18. Poole PH, Sciortino F, Grande T, Stanley HE, Angell CA (1994) Effect of hydrogen bonds on the thermodynamic behavior of liquid water. *Phys Rev Lett* 73(12):1632–1635.
19. Sastry S, Debenedetti PG, Sciortino F, Stanley HE (1996) Singularity-free interpretation of the thermodynamics of supercooled water. *Phys Rev E Stat Phys Plasmas Fluids Relat Interdiscip Topics* 53(6):6144–6154.
20. Adam G, Gibbs JH (1965) On the temperature dependence of cooperative relaxation properties in glass-forming liquids. *J Chem Phys* 43(1):139–146.
21. Limmer DT, Chandler D (2013) Corresponding states for mesostructure and dynamics of supercooled water. *Faraday Discuss* 167:485–498.
22. Murphy DM, Koop T (2005) Review of the vapour pressures of ice and supercooled water for atmospheric applications. *Q J R Meteorol Soc* 131(608):1539–1565.
23. Mishima O, Stanley HE (1998) The relationship between liquid, supercooled and glassy water. *Nature* 396(6709):329–335.
24. Chen S-H, et al. (2006) The violation of the Stokes-Einstein relation in supercooled water. *Proc Natl Acad Sci USA* 103(35):12974–12978.
25. Mallamace F, et al. (2006) The fragile-to-strong dynamic crossover transition in confined water: Nuclear magnetic resonance results. *J Chem Phys* 124(16):161102.
26. Xu Y, et al. (2016) A nanosecond pulsed laser heating system for studying liquid and supercooled liquid films in ultrahigh vacuum. *J Chem Phys* 144(16):164201.
27. Broughton JQ, Gilmer GH, Jackson KA (1982) Crystallization rates of a Lennard-Jones liquid. *Phys Rev Lett* 49(20):1496–1500.
28. Cahn JW, Hillig WB, Sears GW (1964) Molecular mechanism of solidification. *Acta Metall* 12(12):1421–1439.
29. García Fernández R, Abascal JLF, Vega C (2006) The melting point of ice I_h for common water models calculated from direct coexistence of the solid-liquid interface. *J Chem Phys* 124(14):144506.
30. Price WS, Ide H, Arata Y (1999) Self-diffusion of supercooled water to 238 K using PGSE NMR diffusion measurements. *J Phys Chem A* 103(4):448–450.
31. Dash JG, Rempel AW, Wettlaufer JS (2006) The physics of premelted ice and its geophysical consequences. *Rev Mod Phys* 78(3):695–741.
32. Pruppacher HR (1967) Interpretation of experimentally determined growth rates of ice crystals in supercooled water. *J Chem Phys* 47(5):1807–1813.
33. Shikhov AA, Zheltov MA, Korolev AA, Kazakov AA, Leonov AA (2005) Crossover from diffusion-limited to kinetics-limited growth of ice crystals. *J Cryst Growth* 285(1–2):215–227.
34. Buttersack T, Bauerecker S (2016) Critical radius of supercooled water droplets: On the transition toward dendritic freezing. *J Phys Chem B* 120(3):504–512.
35. Safarik DJ, Meyer RJ, Mullins CB (2003) Thickness dependent crystallization kinetics of sub-micron amorphous solid water films. *J Chem Phys* 118(10):4660–4671.
36. Jackson KA, Uhlmann DR, Hunt JD (1967) On the nature of crystal growth from the melt. *J Cryst Growth* 1(1):1–36.
37. Choi S, Jang E, Kim JS (2014) In-layer stacking competition during ice growth. *J Chem Phys* 140(11):014701.
38. Rozmanov D, Kusalik PG (2012) Anisotropy in the crystal growth of hexagonal ice, I_h . *J Chem Phys* 137(9):094702.
39. Weiss VC, Rullich M, Köhler C, Frauenheim T (2011) Kinetic aspects of the thermostatted growth of ice from supercooled water in simulations. *J Chem Phys* 135(3):034701.
40. English NJ (2014) Massively parallel molecular-dynamics simulation of ice crystallisation and melting: The roles of system size, ensemble, and electrostatics. *J Chem Phys* 141(23):234501.
41. Nada H, Furukawa Y (1996) Anisotropic growth kinetics of ice crystals from water studied by molecular dynamics simulation. *J Cryst Growth* 169(3):587–597.
42. Nistor RA, Markland TE, Berne BJ (2014) Interface-limited growth of heterogeneously nucleated ice in supercooled water. *J Phys Chem B* 118(3):752–760.
43. Hudait A, Qiu S, Lupi L, Molinero V (2016) Free energy contributions and structural characterization of stacking disordered ices. *Phys Chem Chem Phys* 18(14):9544–9553.
44. Rozmanov D, Kusalik PG (2011) Temperature dependence of crystal growth of hexagonal ice (I_h). *Phys Chem Chem Phys* 13(34):15501–15511.
45. Nascimento ML, Zanutto ED (2010) Does viscosity describe the kinetic barrier for crystal growth from the liquidus to the glass transition? *J Chem Phys* 133(17):174701.
46. Ngai KL, Magill JH, Plazek DJ (2000) Flow, diffusion and crystallization of supercooled liquids: Revisited. *J Chem Phys* 112(4):1887–1892.
47. Mapes MK, Swallen SF, Ediger MD (2006) Self-diffusion of supercooled *o*-terphenyl near the glass transition temperature. *J Phys Chem B* 110(11):507–511.
48. Smith RS, Kay BD (1999) The existence of supercooled liquid water at 150 K. *Nature* 398:788–791.
49. Amann-Winkel K, et al. (2013) Water's second glass transition. *Proc Natl Acad Sci USA* 110(44):17720–17725.
50. Swallen SF, Traynor K, McMahon RJ, Ediger MD, Mates TE (2009) Self-diffusion of supercooled tris-naphthylbenzene. *J Phys Chem B* 113(14):4600–4608.
51. Sun Y, Xi H, Ediger MD, Yu L (2008) Diffusionless crystal growth from glass has precursor in equilibrium liquid. *J Phys Chem B* 112(3):661–664.
52. Hill CR, et al. (2016) Neutron scattering analysis of water's glass transition and micropore collapse in amorphous solid water. *Phys Rev Lett* 116(21):215501.
53. Shephard JJ, Salzmann CG (2016) Molecular reorientation dynamics govern the glass transitions of the amorphous ices. *J Phys Chem Lett* 7(12):2281–2285.
54. Starr FW, et al. (2001) Thermodynamic and structural aspects of the potential energy surface of simulated water. *Phys Rev E Stat Nonlin Soft Matter Phys* 63(4 Pt 1):041201.
55. Pallares G, et al. (2014) Anomalies in bulk supercooled water at negative pressure. *Proc Natl Acad Sci USA* 111(22):7936–7941.
56. Ediger MD, Harrowell P (2012) Perspective: Supercooled liquids and glasses. *J Chem Phys* 137(8):080901.
57. Gillen KT, Douglass DC, Hoch JR (1972) Self-diffusion in liquid water to -31 C. *J Chem Phys* 57(12):5117–5119.
58. Stevenson KP, Kimmel GA, Dohnálek Z, Smith RS, Kay BD (1999) Controlling the morphology of amorphous solid water. *Science* 283(5407):1505–1507.
59. Kimmel GA, Dohnálek Z, Stevenson KP, Smith RS, Kay BD (2001) Control of amorphous solid water morphology using molecular beams—II: Ballistic deposition simulations. *J Chem Phys* 114:5295–5303.
60. Kimmel GA, Stevenson KP, Dohnálek Z, Smith RS, Kay BD (2001) Control of amorphous solid water morphology using molecular beams—I: Experimental results. *J Chem Phys* 114:5284–5294.
61. Dohnálek Z, Kimmel GA, Ayotte P, Smith RS, Kay BD (2003) The deposition angle-dependent density of amorphous solid water films. *J Chem Phys* 118(1):364–372.
62. Smith RS, et al. (2003) Molecular beam studies of nanoscale films of amorphous solid water. *Water in Confining Geometries, Cluster Physics*, eds Buch V, Devlin JP (Springer, Berlin), pp 337–357.
63. Kimmel GA, Petrik NG, Dohnálek Z, Kay BD (2005) Crystalline ice growth on Pt(111): Observation of a hydrophobic water monolayer. *Phys Rev Lett* 95(16):166102.
64. Kimmel GA, Petrik NG, Dohnálek Z, Kay BD (2006) Layer-by-layer growth of thin amorphous solid water films on Pt(111) and Pd(111). *J Chem Phys* 125(4):44713.
65. Kimmel GA, Petrik NG, Dohnálek Z, Kay BD (2007) Crystalline ice growth on Pt(111) and Pd(111): Nonwetting growth on a hydrophobic water monolayer. *J Chem Phys* 126(11):114702.
66. Carr THG, Shephard JJ, Salzmann CG (2014) Spectroscopic signature of stacking disorder in ice I. *J Phys Chem Lett* 5(14):2469–2473.
67. Thurmer K, Bartelt NC (2008) Growth of multilayer ice films and the formation of cubic ice imaged with STM. *Phys Rev B* 77(19):195425.
68. Thurmer K, Bartelt NC (2008) Nucleation-limited dewetting of ice films on Pt(111). *Phys Rev Lett* 100(18):186101.
69. Kumar P, Stanley HE (2011) Thermal conductivity minimum: A new water anomaly. *J Phys Chem B* 115(48):14269–14273.
70. Jenniskens P, Banham SF, Blake DF, McCoustra MRS (1997) Liquid water in the domain of cubic crystalline ice Ic. *J Chem Phys* 107(4):1232–1241.
71. Dohnálek Z, et al. (2000) The effect of the underlying substrate on the crystallization kinetics of dense amorphous solid water films. *J Chem Phys* 112(13):5932–5941.
72. Safarik DJ, Mullins CB (2003) A new methodology and model for characterization of nucleation and growth kinetics in solids. *J Chem Phys* 119(23):12510–12524.
73. Hage W, Hallbrucker A, Mayer E (1994) Crystallization kinetics of water below 150 K. *J Chem Phys* 100:2743–2747.
74. Hage W, Hallbrucker A, Mayer E, Johari GP (1995) Kinetics of crystallizing D_2O water near 150 K by Fourier-transform infrared-spectroscopy and a comparison with the corresponding calorimetric studies on H_2O water. *J Chem Phys* 103(2):545–550.
75. Jenniskens P, Blake DF (1996) Crystallization of amorphous water ice in the solar system. *Astrophys J* 473(2 Pt 1):1104–1113.
76. Handle PH, Loerting T (2016) Dynamics anomaly in high-density amorphous ice between 0.7 and 1.1 GPa. *Phys Rev B* 93(6):064204.
77. Avrami M (1939) Kinetics of phase change. I. *J Chem Phys* 7:1103–1112.
78. Avrami M (1940) Kinetics of phase change. II. *J Chem Phys* 8:212–224.
79. Jackson KA (2004) *Kinetic Processes: Crystal Growth, Diffusion, and Phase Transitions in Materials* (Wiley-VCH, Weinheim, Germany).
80. Hallett J (1964) Experimental studies of the crystallization of supercooled water. *J Atmos Sci* 21(6):671–682.
81. Hobbs PV (1974) *Ice Physics* (Oxford Univ Press, Oxford).
82. McClure SM, et al. (2006) Transport in amorphous solid water films: Implications for self-diffusivity. *J Phys Chem B* 110(36):17987–17997.